*Fibers and Polymers* 2018, Vol.19, No.1, 1-10
DOI 10.1007/s12221-018-7305-6

ISSN 1229-9197 (print version)
ISSN 1875-0052 (electronic version)

# Miscibility, Crystallization Behaviors and Toughening Mechanism of Poly(butylene terephthalate)/Thermoplastic Polyurethane Blends

**Yanping Hao, Huili Yang, Huiliang Zhang*, and Zhishen Mo**

*Key Laboratory of Polymer Ecomaterials, Chinese Academy of Sciences, Changchun Institute of Applied Chemistry, Changchun 130022, P. R. China*

(Received March 28, 2017; Revised October 13, 2017; Accepted November 9, 2017)

**Abstract:** Blends of poly(butylene terephthalate) (PBT)/thermoplastic polyurethane (TPU) were prepared by melt compounding. The miscibility, crystallization behaviors and toughening mechanism of the PBT/TPU blends were studied. Dynamic mechanical analysis results demonstrated that PBT was immiscible with TPU. Differential scanning calorimetry and wide angle X-ray diffraction results showed that the crystallinity of PBT decreased with increasing TPU content. Furthermore, blending with TPU did not modify the crystal structure of PBT. The small angle X-ray scattering results indicated that the crystal layer thickness decreased and the amorphous layer thickness increased with increasing TPU content, indicating that TPU mainly resided in the interlamellar region of PBT spherulites in the blends. An obvious improvement in toughness of PBT was achieved with addition of TPU. Neat PBT had elongation at break and impact strength of about 15 % and 2.9 kJ/m$^2$, respectively. However, the elongation at break and impact strength of the 70/30 PBT/TPU blend reached 410 % and 62.9 kJ/m$^2$, respectively. The morphology of the PBT/TPU blends after tensile and impact tests was investigated, and the corresponding toughening mechanism is discussed. It was found that the PBT showed obvious shear yielding in the blend during the tensile and impact tests, which induced dissipation of energy and, therefore, led to the improvement in toughness of the PBT/TPU blends.

**Keywords:** Poly(butylene terephthalate), Thermoplastic polyurethane, Miscibility, Crystallization behaviors, Toughening mechanism

## Introduction

Semi-crystalline poly(butylene terephthalate) (PBT) is an important engineering thermoplastic with good properties of chemical resistance, electric insulation, lubricity and processability; it has been widely used in the automotive and constructional industry. It also exhibits high rates of crystallization [1], which allow short cycle times in injection molding. However, it generally suffers strong limitations in its end use when both toughness and high impact resistance are required. The toughening of PBT has been studied for a long time and numerous attempts to improve its mechanical toughness by blending other polymers with PBT have been described. Blending polymers used have been polyolefin [2], polycarbonate [3-8], polyamide [9-11], polyarylate [12,13], polyesters [14], and acrylonitrile-butadiene-styrene (ABS) terpolymers [15-17]. Elastomeric polymers, such as styrene-b-ethylene/butylene-b-styrene triblock copolymer (SEBS) [18], ethylene-propylene-diene rubber (EPDM) [19] and ethylene propylene rubber (EPR) [20] have also been employed for modifying polyesters.

As examples, Hage *et al.* [15] studied the effect of ABS type, extrusion temperature, extrusion type, molding conditions and PBT type on the notched impact strength of PBT/ABS blends in detail, and PBT/ABS blends with high notched impact strength were obtained. Larocca *et al.* [21] reported improvements in the toughness of PBT by blending with acrylonitrile-EPDM (ethylene/propylene/diene elastomer)-styrene (AES). It was found that a supertough blend could be achieved with at least 30 wt% of AES in PBT using an appropriate molding temperature. Sharma *et al.* [18] investigated a styrene-b-ethylene/butylene-b-styrene triblock copolymer (SEBS) as well as the SEBS polymer grafted with maleic anhydride (MA) (SEBS-g-MA) employed as impact modifiers. They found the normalized notched impact strength increased with addition of SEBS content and the SEBS-g-MA could further enhance the toughness due to the interphase adhesion.

Thermoplastic polyurethanes (TPU) have a unique combination of toughness, durability, flexibility, biocompatibility and biostability that makes them suitable materials for use in a diverse range of implantable medical devices [22-25]. Technically, it is a thermoplastic elastomer consisting of linear, segmented block copolymers composed of hard and soft segments. The hard segments are based on diisocyanates and short diol or diamine, and the soft segments consist of either long polyether or polyester glycols. In the process of coating solidification, and injection or extrusion molding, microphase separation always occurs because of the immiscibility of the hard segments with the soft segments. The hard segments of different molecules are connected with each other by intermolecular hydrogen bonds (H-bonds) and form domains to act as multifunctional tie points functioning both as physical crosslinks and reinforcing fillers, while the soft segments form an elastomer matrix which accounts for the elastic properties of TPU [26-28]. The chemical structures of the hard and soft segments for TPU are shown in Scheme 1. It usually behaves as a toughening agent to improve the impact properties of a brittle polymer because the elastomeric

*Corresponding author: hlzhang@ciac.ac.cn

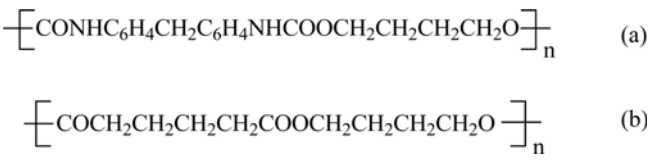

**Scheme 1.** The structures of (a) hard segments and (b) soft segments for TPU.

polyurethane behaves either as dispersed particles or is dissolved in these blends [29]. Palanivelu *et al.* [30] used TPU to toughen PBT and they found that the impact strength of the blend with 30 wt% TPU increased by nearly 10 times. They also studied the instrumented impact strength of the blends. The blend with 5 wt% TPU was the optimum blend with respect to instrumented impact strength. They also studied the rheological properties. However, miscibility, crystallization behaviors and toughening mechanisms of PBT/TPU blends have not been further investigated to our knowledge. Thus, we choose TPU as a toughener to toughen PBT and investigate the miscibility, crystallization behaviors, and toughening mechanisms of the PBT/TPU blends.

## Experimental

### Materials

The PBT used in this work is a commercial product of Yizheng Chemical Fiber Group, China. The MFI is 7.8 g/10 min (240 °C). The TPU (trade name EX85A with a $M_w$ of 35,000 g/mol) used is ester based and obtained from Beijing Gzlchem Technology Co., Ltd., China. The density of the TPU is 1.19 g/cm. PBT and TPU were dried in a vacuum oven for 8 h at 80 °C to remove absorbed water before blending.

### Sample Preparation

Blends of PBT/TPU were prepared by melt mixing using a Haake batch intensive mixer (Haake Rheomix 600, Germany) at 50 rpm and 240 °C for 5 min. The mixing compositions of the PBT/TPU blends were 100/0, 90/10, 80/20, and 70/30 w/w. After blending, all the samples were cooled to room temperature under atmosphere air. Sheets were prepared using a hot press at 240 °C, a hold pressure of 6 MPa and a hold time of 5 min, followed by quenching to room temperature between two thick-metal blocks kept at room temperature. A template frame was used to ensure a constant sheet thickness of 4.0 mm for the impact tests and 1.0 mm for the tensile tests, and care was taken to ensure the same thermal history of all sheets. The specimens were then sealed in plastic bags awaiting the processing and analysis.

### Characterization and Analysis

Misibility of the blends was studied by dynamic mechanical analysis (DMA) (TA Instruments Co., DMA, Q800, USA). The compression-molded PBT/TPU samples were sized 20 mm×4 mm×1 mm. The experiment was carried out in tension mode at a constant heating rate of 3 °C/min and a frequency of 1 Hz, from -80 to 120 °C.

Thermal properties of the blends were studied by differential scanning calorimetry (DSC) (TA Instruments Co., DSC Q20, USA) on specimens sliced from the compression molded samples. Samples (about 5-8 mg) were placed and sealed in aluminum pans. The samples were then heated first from -60 up to 250 °C at 10 °C/min (the first heating scan) and held at 250 °C for 5 min to eliminate their previous thermal history. Following that, the samples were cooled to -60 °C at the same rate and then heated again finally (the second heating scan).

Wide angle X-ray diffraction (WAXD) patterns were recorded using a Rigaku model Dmax 2500 X-ray diffractometer. WAXD patterns were recorded from 0 ° to 40 ° at 4 °/min. The Cu $K_\alpha$ radiation ($\lambda$=0.154 nm) source was operated at 40 kV and 30 mA. Before testing, the samples were prepared using a hot press at 250 °C and a hold time of 5 min, followed by annealing at 190 °C for 1 h.

Small angle X-ray scattering (SAXS) experiments of specimens were performed at RT using a NanoSTAR-U (Bruker AXS Inc., Germany) with Cu $K_\alpha$ radiation (wavelength, $\lambda$=0.154 nm). The generator was operated at 40 kV and 650 μA. Two-dimensional SAXS patterns were obtained using a HI-STAR detector. The sample-to-detector distance was $L_{SD}$=1074 mm. The effective scattering vector $q$ [$q=(4\pi/\lambda)\sin\theta$, where $\theta$ is the scattering angle] at this distance ranged from 0.044 to 2.0 $nm^{-1}$. The X-ray exposure time was 60 min. For the SAXS measurements, corrections were made for instrumental background. Before testing, the samples were prepared using a hot press at 250 °C and a hold time of 5 min, followed by annealing at 190 °C for 1 h.

The uniaxial tensile tests were carried out at room temperature on an Instron 1121 testing machine (Instron Co., USA). Specimens (20 mm×4 mm×1 mm) were cut from the previously compression-molded sheet into a dumbbell shape. The measurements were conducted at a cross-head speed of 20 mm/min at room temperature according to ASTM D638-2008. At least five runs for each sample were measured, and the results were averaged.

Notched Izod impact tests were performed at room temperature according to ASTM D256-2010 on an impact testing machine (Changchun City Intelligent Instrument Equipment Co., Ltd., China). The samples, with dimensions 63.2 mm×12.0 mm×4.0 mm, were obtained from compression-molded specimens. The notch was milled in, having a depth of 2.54 mm, an angle of 45 ° and a notch radius of 0.25 mm.

The fracture surfaces from the tensile and impact tests of PBT/TPU blends were characterized by scanning electron microscopy (XL-30 ESEM FEG, FEI Co., USA). The samples were fractured after immersion in liquid nitrogen for about 5 min. A layer of gold was sputter-coated uniformly

over all of the fractured surfaces before SEM observations.

## Results and Discussion

### Miscibility

DMA is an effective method to investigate the miscibility of blends. The influence of TPU on the loss factor (tan$\delta$) and the storage modulus ($E'$) of the PBT is shown in Figure 1. As observed from Figure 1(a), the variations of tan$\delta$ as a function of temperature, neat PBT exhibited a single relaxation peak at approximately 60 °C, corresponding to its glass transition temperature ($T_g$). For neat TPU, a well-resolved peak was observed at approximately -17 °C, corresponding to its glass transition. In case of the blends, the tan$\delta$ curves revealed two glass transition temperatures, the higher $T_g$ corresponding to the PBT component, and the lower one corresponding to TPU component. Moreover, the $T_g$ of both PBT and TPU components did not shift toward each other when the blend composition was varied, indicating that PBT and TPU were immiscible. However, one should notice that the $T_g$ of TPU component in the blend shifted toward lower temperature compared to neat TPU, although the $T_g$ of PBT component in the blend was nearly unchanged with varying TPU contents. This behavior indicated that PBT and TPU were completely immiscible.

Figure 1(b) shows the variations of the storage modulus ($E'$) as a function of temperature for the blends with different TPU content. The $E'$ of the blend gradually decreased with increasing TPU content particularly for 80/20 and 70/30 blends, indicating an increase in the flexibility of PBT imparted by TPU. The decrease in the $E'$ of the PBT/TPU blends could be attributed to the low stiffness of the TPU. Moreover, $E'$ decreased rapidly at about 50 °C for all samples except pure TPU because of the glass transition of PBT.

Likewise, the differential solubility parameter, defined as the difference between the solubility parameters of the components of the blend, was often used to estimate the miscibility of two components. According to this concept, if two polymers were thermodynamically miscible, the critical differential solubility parameter should not exceed 0.5. The solubility parameter of PBT is 10.8 [31]. The solubility parameters of the hard segments and soft segments for TPU are 23.5 and 19.4, respectively [32]. Thus, the difference in the solubility parameters of the hard segments of TPU and

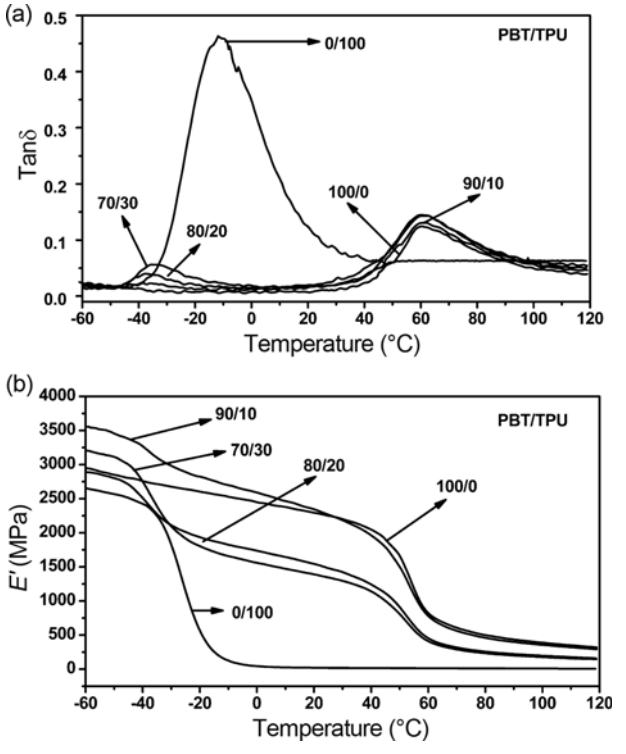


**Figure 1.** (a) Tan$\delta$ and (b) storage modulus for neat PBT and PBT/TPU blends.

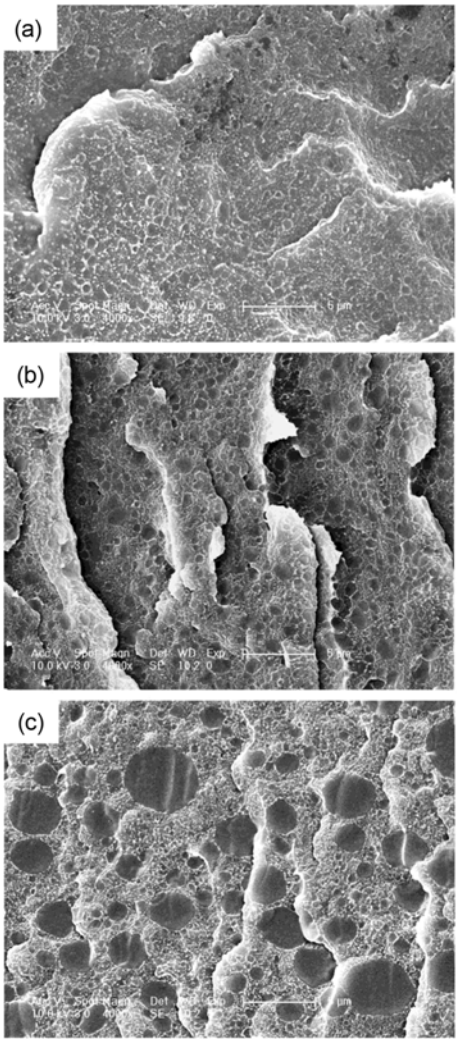


**Figure 2.** SEM micrographs of cryo-fractured surfaces of PBT/TPU blends; (a) 90/10, (b) 80/20, and (c) 70/30.

PBT was 12.7, and the difference in the solubility parameters of the soft segments of TPU and PBT was 8.6. These results indicated that PBT and TPU were immiscible, in agreement with the DMA results.

**Morphology**

It is well recognized that the properties of a polymer blend are strongly influenced by its morphology. Figure 2 presents the SEM micrographs of cryo-fractured surfaces of PBT/TPU blends. In Figure 2, it was found that all the blends consisted of a clear phase-separated morphology, which was in agreement with the two $T_g$s obtained from the DMA measurements. The blends displayed fine dispersion of the TPU minor phase in the PBT matrix. A further increase in the TPU content led to a further increase in the average particle size.

**Crystallization and Melting Behaviors**

The nonisothermal melt crystallization and subsequent melting of neat PBT and PBT/TPU blends were observed by DSC. Figure 3 shows the DSC thermograms of the first cooling trace and second heating trace; and the corresponding parameters derived from the DSC curves are summarized in Table 1. The crystallinity of the samples was evaluated from the heat evolved during crystallization by equation (1):

$$x_c = \frac{\Delta H_f}{w_{PBT} \times \Delta H_f^0} \times 100\% \quad (1)$$

where $\Delta H_f$ is the heat of fusion, $\Delta H_f^0$ is the heat of fusion for 100% crystalline PBT (142 J/g) [33] and $w_{PBT}$ is the weight fraction of PBT.

In the case of neat PBT, a crystallization peak temperature ($T_c$) was observed at 192.2 °C, and the crystallization proceeded in a narrow temperature range, as shown in Figure 3(a). As for the PBT/TPU blends, the PBT crystallization peak became broader and shifted to a lower temperature. The peak area was obviously smaller than that of neat PBT. From the observations, it could be concluded that the incorporation of TPU retarded the nonisothermal melt crystallization of the PBT matrix, a behavior also reported by Hage *et al.* for PBT/AES blends [15]. In addition, the $\Delta H_c$ decreased gradually with increasing TPU content, as listed in Table 1.

Figure 3(b) shows the subsequent melting trace of neat PBT and PBT/TPU blends after cooling from the melt at 10 °C/min (second heating). As observed in Figure 3(b), neat PBT and PBT/TPU blends showed double melting peaks. The small melting peak we attribute to the melting of the less perfect crystals, possibly formed during heating. The second main melting peak is attributed to the melting of the original and recrystallized crystals [34]. The peaks at low temperature were at 10 °C lower than the peak at high temperature. Similar results were also observed previously by Sun *et al.* [32] PBT is one of the fast crystallizing polymers and the crystallization kinetics have been only partially investigated [35]. PBT is known to possess two crystalline structures, $\alpha$ and $\beta$ forms, which can undergo a reversible transformation at a low level of applied stress [36]. The appearance of double melting peaks could be interpreted reasonably as the result of sequential melting of

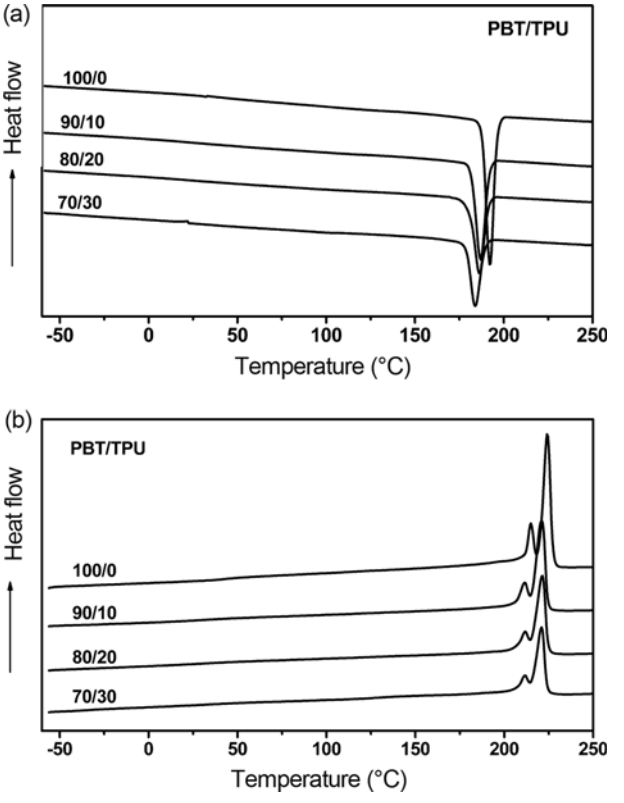


**Figure 3.** DSC thermograms recorded for neat PBT and PBT/TPU blends; (a) first cooling and (b) second heating.

**Table 1.** Crystallization parameters for neat PBT and PBT/TPU blends

| PBT/TPU (w/w) | $T_c$ (°C) | $\Delta H_c$ (J/g) | $T_{m1}$ (°C) | $T_{m2}$ (°C) | $\Delta H_f$ (J/g) | $W_{c,h}$ (%) | $W_{c,x}$ (%) |
|---|---|---|---|---|---|---|---|
| 100/0 | 192.2 | 63.0 | 214.8 | 224.2 | 48.4 | 34.1 | 45.7 |
| 90/10 | 186.9 | 50.4 | 211.0 | 221.3 | 35.8 | 28.0 | 43.4 |
| 80/20 | 186.3 | 44.8 | 211.2 | 221.5 | 29.3 | 25.8 | 42.3 |
| 70/30 | 183.9 | 38.0 | 211.5 | 221.1 | 23.5 | 23.6 | 37.4 |

$W_{c,h}$ obtained from DSC and $W_{c,x}$ obtained from WAXD.

the two different forms of the crystalline polymer. PBT is a highly crystalline polymer that could crystallize rapidly even under a quenched condition. The two melting temperatures tended to shifting lower temperatures with addition of 10 wt% TPU content, as shown in Figure 3(b). However, a further increase in the TPU content, the two melting temperatures remained constant. These results indicated that the addition of TPU content restricted the mobility of PBT chains leading to the limitation of the recrystallization-remelting process in the second heating stage. Moreover, the melting enthalpy ($\Delta H_f$) and crystallinity (in Table 1) of PBT/TPU blends went to decrease with increasing TPU content. This lower $\Delta H_f$ of PBT/TPU blends was a positive outcome. It indicated that less amount of heat would be required during the processing of these blends.

**Analysis by WAXD and SAXS**

Figure 4 shows the WAXD patterns for the neat PBT and PBT/TPU blends. It was found that PBT showed seven crystalline peaks at $2\theta_{0\bar{1}1}$=15.9 °, $2\theta_{010}$=17.1 °, $2\theta_{\bar{1}02}$=20.6 °, $2\theta_{100}$=23.3 °, $2\theta_{\bar{1}11}$=25.1 °, $2\theta_{\bar{1}\bar{1}2,\ 012,\ 101}$=29.3 °, $2\theta_{1\bar{2}1,\ 1\bar{2}0,\ 120}$= 31.3 °, and one amorphous peak at $2\theta_{\alpha}$=21.9 °. For the PBT/TPU blends, the similar diffraction peaks could be observed due to no crystalline peak in TPU content. The positions of the diffraction remained unchanged in the blends compared with the neat PBT, which indicated that there was no variation of the cell parameters. In brief, blending with TPU did not modify the crystal structure of PBT in the PBT/TPU blends.

According to the graphic multipeak resolution method [37], the crystallinity of neat PBT and PBT/TPU blends were determined and was calculated by equation (2) [38,39]:

$$W_{c,x} = \frac{\sum_i C_{i,hkl}(\theta) I_{i,hkl}(\theta)}{\sum_i C_{i,hkl}(\theta) I_{i,hkl}(\theta) + k_i C_a(\theta) I_a(\theta)} \times 100\% \quad (2)$$

where $W_{c,x}$ is the crystallinity, $I_{i,hkl}(\theta)$ and $I_a(\theta)$ are the relative intensities of the crystalline and amorphous peaks, respectively, and $C_{i,hkl}(\theta)$ and $C_a(\theta)$ are the correction factors of the crystalline and amorphous peaks, respectively. On the basis of the X-ray diffraction intensity theory, $K$ is the total correction factor, the calibration constant [$K=C_a(\theta)\times k_i$, where $k_i$ is the relative scattering coefficient, which is a ratio of calculated diffraction intensity ($\sum I_{i,cal}$) to total scattering intensity ($\sum I_{i,total}$) for unit weight of crystalline polymer, and $k_i=(\sum I_{i,cal}/\sum I_{i,total}\ \ (k_i \le 1))$]. Here, $C_{i,hkl}(\theta)$ and $C_a(\theta)$ could be calculated by equation (3):

$$C_{i,hkl(\theta)}^{-1} \text{ or } C_a^{-1}(\theta) = f^2 \cdot \frac{1+\cos^2 2\theta}{\sin^2\theta \cdot \cos\theta} \cdot e^{-2B(\sin\theta/\lambda)^2}$$

$$= \sum_i N_i f_i^2 \cdot \frac{1+\cos^2 2\theta}{\sin^2\theta \cdot \cos\theta} \cdot e^{-2B(\sin\theta/\lambda)^2} \quad (3)$$

where $f$ is the atomic scattering factor for one crystallographic structural repeating unit, $f_i$ is the scattering factors of the $i$th atom, $N_i$ is the number of $i$th atoms in a repeating unit, $2\theta$ is the Bragg angle, the angle factor ($LP$)=($1+\cos^2 2\theta$)/$\sin^2\theta\cos\theta$, the temperature factor ($T$)= $e^{-2B(\sin\theta/\lambda)^2}$, and $2B$=10.

$f_i$ could be expressed approximately by equation (4):

$$f_i(\sin\theta/\lambda) = \sum_{i=1}^{4} a_i \cdot e^{-b_i(\sin\theta/\lambda)^2} + C \quad (4)$$

where the values of $a$, $b$, and $C$ are given in books for Macgillavry *et al.* [40].

The total WAXD curve of 80/20 PBT/TPU blend was resolved into crystalline and amorphous portions (Figure 5). From equations (2)-(4), the X-ray diffraction data of 80/20 PBT/TPU blend is summarized in Table 2. $I_{hkl}=C_{i,hkl}(\theta)I_{i,hkl}(\theta)$ or $C_a(\theta)I_a(\theta)$ is the integrating intensity scattered over a suitable angular interval by the crystalline and the amorphous phases, respectively. There were 12 atoms of carbon, 12 atoms of hydrogen, and 4 atoms of oxygen in a repeating unit of PBT; the total atomic scattering factor was $f_{hkl}^2 = 12f_C^2 + 12f_H^2 + 4f_O^2$, where $k_i$=0.9, $C_a(\theta)$=1.0, $K$= $k_iC_a(\theta)$=0.9. With the data of Table 2, equation (2) could be reduced to give equation (5):

$$W_{c,x} = \frac{0.41I_{0\bar{1}1} + 0.51I_{010} + 0.85I_{\bar{1}02} + 1.25I_{100} + 1.62I_{\bar{1}11} + 2.73I_{\bar{1}\bar{1}2,012,101} + 3.57I_{1\bar{2}1,1\bar{2}0,120}}{0.41I_{0\bar{1}1} + 0.51I_{010} + 0.85I_{\bar{1}02} + 1.25I_{100} + 1.62I_{\bar{1}11} + 2.73I_{\bar{1}\bar{1}2,012,101} + 3.57I_{1\bar{2}1,1\bar{2}0,120} + 2.40I_a} \times 100\% \quad (5)$$

where $I_a$ is the intensity of amorphous peak. With equation (5), the crystallinity ($W_{c,x}$) of neat PBT and PBT/TPU blends were determined by WAXD and shown in Table 1. The crystallinity of the 70/30 PBT/TPU blend decreased by 37.4 %, whereas that of neat PBT was 45.7 %. The crystallinity values in Table 1 exhibit the order $W_{c,x} > W_{c,h}$. The crystallinity determined from X-ray diffraction ($W_{c,x}$) was equal to the sum of the crystalline and interphase contents, while the measurement of fusion enthalpy by calorimetry ($W_{c,h}$) yields values which was equal to the crystalline content. Imperfections of crystals were not easily distinguished from the amorphous phase. Therefore, some

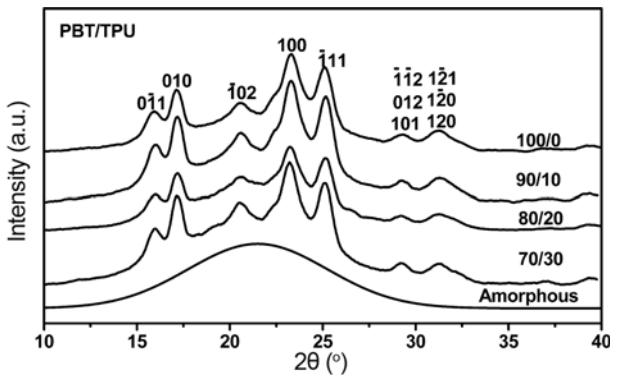


**Figure 4.** WAXD patterns of neat PBT and PBT/TPU blends.

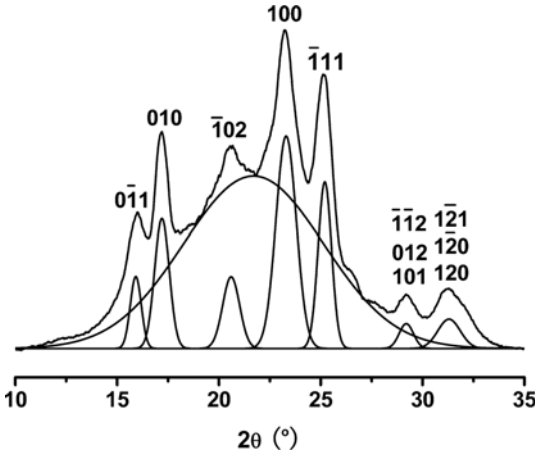


**Figure 5.** Resolution of the WAXD curve of 80/20 PBT/TPU blend into crystalline and amorphous portions.

disagreements among the quantitative results of crystallinity by different measurement methods were frequently encountered [41]. The crystallinity was closely related to the impact strength and elongation at break for the PBT/TPU blends. In order to improve the impact strength, the optimal TPU content was 30 wt%, and the degree of crystallinity was 37.4 % for the PBT/TPU blends.

SAXS was used to investigate the crystal structure and macrostructure of neat PBT before and after blending with TPU. Figure 6 shows the Lorentz-corrected SAXS curves of the blends at various compositions annealed at 190 °C for 1 h. The long spacing $d_{ac}$, which was defined as the crystal layer thickness together with one interlamellar amorphous layer, measured along the lamella normal and calculated using Bragg equation (6) [42]. The crystal layer thickness $d_c$ and the amorphous layer thickness $d_a$ could be calculated using equations (7) and (8), respectively.

$$d_{ac} = \frac{2\pi}{q_{\max}} \tag{6}$$

$$d_c = d_{ac} \times W_{c,h} \tag{7}$$

$$d_a = d_{ac} - d_c \tag{8}$$

here $q_{\max}$ represents the position of the intensity maximum in a SAXS pattern, $W_{c,h}$ represents the crystallinity of the samples, which is derived from DSC measurement (Table 1). The obtained $q_{\max}$, $d_{ac}$, $d_c$ and $d_a$ values are summarized in Table 3. In Figure 6, neat PBT exhibited a broader scattering peak could be observed around $q$=0.3-0.5 nm$^{-1}$. The scattering peaks gradually shifted in position to lower $q$ values with increasing TPU content, which indicated the $d_{ac}$ values gradually increased. In Table 3, the $d_{ac}$, $d_c$ and $d_a$ values were 14.3, 4.9, and 9.4 nm, respectively, for neat PBT. For the 70/30 PBT/TPU blend, they became 17.0, 2.0, and 15.0 nm, respectively. It was obvious that all of values of $d_{ac}$ and $d_a$ increased and the $d_c$ values decreased with increasing TPU

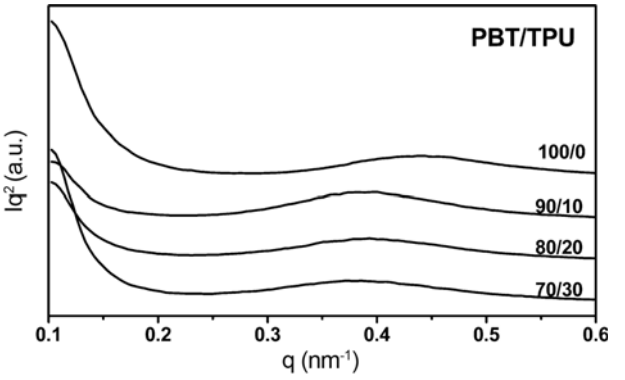


**Figure 6.** Lorentz-corrected SAXS curves of neat PBT and PBT/TPU blends.

**Table 3.** SAXS values of neat PBT and PBT/TPU blends

| PBT/TPU (w/w) | $q_{\max}$ (nm$^{-1}$) | $d_{ac}$ (nm) | $d_c$ (nm) | $d_a$ (nm) |
|---|---|---|---|---|
| 100/0 | 0.44 | 14.3 | 4.9 | 9.4 |
| 90/10 | 0.40 | 15.7 | 4.4 | 11.3 |
| 80/20 | 0.39 | 16.1 | 4.1 | 12.0 |
| 70/30 | 0.37 | 17.0 | 2.0 | 15.0 |

**Table 2.** X-ray diffraction data of 80/20 PBT/TPU blend

| hkl | A | $0\bar{1}1$ | 010 | $\bar{1}02$ | 100 | $\bar{1}11$ | $\bar{1}\bar{1}2$, 012, 101 | $1\bar{2}1$, $1\bar{2}0$, 120 |
|---|---|---|---|---|---|---|---|---|
| $2\theta$ | 21.7 | 15.9 | 17.2 | 20.6 | 23.3 | 25.2 | 29.2 | 31.3 |
| $I_a(\theta)$ or $I_{i,hkl}(\theta)$ | 5165 | 169 | 455 | 328 | 1033 | 546 | 64 | 133 |
| $I$ | 4645 | 70 | 232 | 280 | 1292 | 884 | 176 | 473 |
| $T$ | 0.86 | 0.92 | 0.91 | 0.87 | 0.84 | 0.81 | 0.77 | 0.74 |
| $f^2 = 12f_H^2 + 12f_C^2 + 4f_O^2$ | 470 | 558 | 538 | 487 | 446 | 417 | 361 | 334 |
| $LP$ | 53.5 | 101.6 | 86.5 | 59.6 | 46.1 | 39.1 | 28.7 | 24.7 |
| $C(\theta)$ | 1.00 | 0.41 | 0.51 | 0.85 | 1.25 | 1.62 | 2.73 | 3.57 |
| $K$ | 0.9 | | | | | | | |

A: amorphous peak.

content. However, the increase in $d_a$ was large. For example, the increase in $d_a$ was around 5.6 nm after blending 30 wt% TPU as compared to that of neat PBT. Such significant increase in $d_a$ suggested that amorphous TPU might destroy the crystalline of PBT and reside in the interlamellar region of PBT spherulites. Similar results were also found in poly(butylene succinate-cobutylene adipate)/poly(vinyl phenol) blends [43].

**Mechanical Properties**

Figure 7 shows the stress-strain curves of neat PBT and PBT/TPU blends, and the corresponding parameters were given in Table 4. Neat PBT was very rigid and brittle, with tensile strength around 52.8 MPa, and the elongation at break only about 15 %. It showed a distinct yield point with subsequent failure by neck instability. In contrast, the PBT/TPU blends showed clear yielding and stable neck growth through cold drawing. The samples were finally broken at a drastically increased elongation and the elongation continuously increased with increasing TPU content. Surprisingly, it was interesting to notice that only at 20 wt% of TPU, a high elongation at break of 159 % was obtained, and the elongation at break reached its maximum (410 %) when 30 wt% TPU was added, as shown in Table 4. Broadening of the yield peaks as well as more visually observable stress whitening in the tensile test specimens were observed for the PBT/TPU blends, as shown in Figure 8. Extensive stress

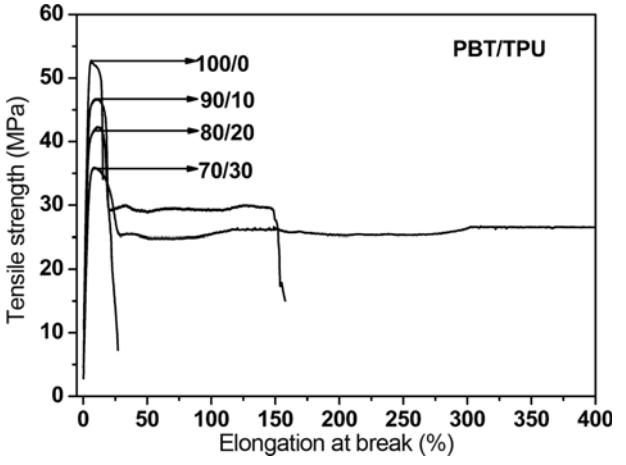


**Figure 7.** Stress-strain curves of neat PBT and PBT/TPU blends.

**Table 4.** Mechanical properties of neat PBT and PBT/TPU blends

| PBT/TPU (w/w) | Young's modulus (MPa) | Tensile strength (MPa) | Elongation at break (%) | Impact strength (kJ/m$^2$) |
|---|---|---|---|---|
| 100/0 | 1340±37 | 52.8±5.6 | 15±0.8 | 2.9±0.1 |
| 90/10 | 1227±30 | 46.7±3.0 | 27±1.5 | 4.4±0.4 |
| 80/20 | 1066±19 | 42.3±2.6 | 159±5.1 | 10.9±1.2 |
| 70/30 | 811±11 | 36.9±1.9 | 410±10.6 | 62.9±6.1 |

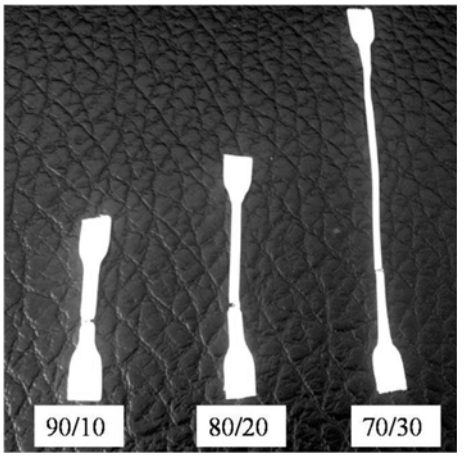


**Figure 8.** Visualization of break behavior of the tensile test specimens of PBT/TPU blends.

whitening of these blends resulted in larger strain at break than neat PBT. The increase in the elongation at break could be attributed to the extensive shear whitening in the test specimens in addition to the low degree of crystallinity of the blends (Table 1) as compared to neat PBT. On the other hand, the tensile strength and modulus of the PBT/TPU blends decreased with increasing TPU content. The tensile strength decreased from 52.8 MPa (neat PBT) to 36.9 MPa (30 wt% TPU), whereas the modulus decreased from 1340 MPa (neat PBT) to 811 MPa (30 wt% TPU), as shown in Table 4. This consequence was expected and could be attributed to the lower yield stress and tensile modulus of the TPU elastomer as compared to those of PBT. The presence of TPU elastomer domains in PBT, acting as stress concentrators, resulted in yielding at an overall stress lower than that of neat PBT. TPU also decreased the crystallinity of the PBT/TPU blends, as evident from Table 1. A lower degree of crystallinity meant a higher content of free volume which led to a decrease in stiffness [44].

The toughening ability of the PBT/TPU blends was also evaluated by notched Izod impact measurements. The impact strength of neat PBT and PBT/TPU blends is shown in Figure 9. The impact strength gradually increased from 2.9 kJ/m$^2$ for neat PBT to 10.9 kJ/m$^2$ for the 80/20 PBT/TPU blend. When 30 wt% TPU was added, the impact strength increased greatly to 62.9 kJ/m$^2$, which was approximately 22 times higher than that of the neat PBT. Wu [45] suggested that the toughness of rubber modified thermoplastics increased as the ligament size (distance between the adjacent rubber particles) was reduced. The interparticle distance or ligament size could be reduced either by increasing the rubber concentration or by decreasing the rubber particle size. The increase in the impact strength at 30 wt% of TPU content could be attributed to decreasing the interparticle distance by increasing the concentration.

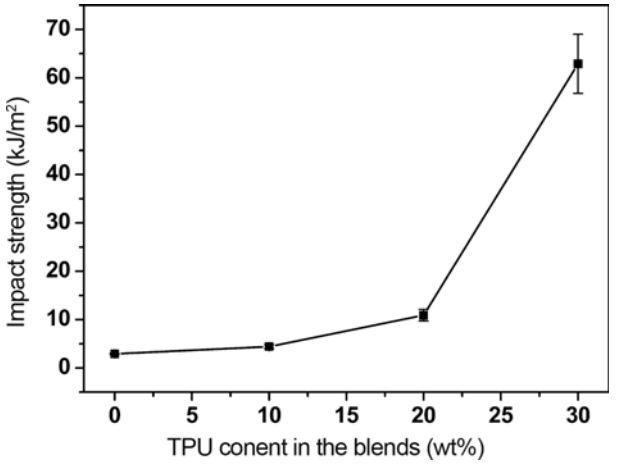


**Figure 9.** Effect of TPU content on the impact strength of PBT/TPU blends.

**Toughening Mechanisms**

To investigate the toughening mechanism of the PBT/TPU blends, the morphology of different necking regions of the tensile specimen was examined by SEM using longitudinal cryofracture. The SEM micrographs of the 80/20 PBT/TPU blend are shown in Figure 10. In Figure 10(a), the different locations in the necking region are marked as B, C, and D, which represent the different stretching stages, namely, the initial, developing, and developed stages, respectively. The corresponding morphological structures are shown in Figures 10(b)-(d). For rubber-toughened plastic systems, two types of cavitations induced by impact or tensile testing have been discriminated: internal cavitations in the rubber domains for the blends with strong interfacial adhesion, and debonding cavitations between the interfaces, when the interfacial adhesion was not sufficient [46-48]. The TPU phase acted as stress concentrators because it had an elastic property that differed from the PBT matrix. The consequent stress concentration led to the development of a triaxial stress in the TPU particles. Because of the lack of phase adhesion, debonding could easily take place at the particle matrix interface perpendicular to the stress direction. Thus, the cavities developed and were clearly observed in the initial stage of the stretching, shown in Figure 10(b). Once the voids were formed, the hydrostatic stress state caused by the stress concentration was released with the stress state in the ligaments of PBT between the voids being converted from a triaxial to more biaxial or uniaxial tensile stress state. With the continuous growth of the voids, weak shear bands formed in the matrix between the TPU particles. At this stage, these cavities were enlarged along the stress direction, as shown in Figure 10(c). With the continuous plastic growth of voids, PBT matrix between the TPU particles deformed more easily and therefore shear yielding was achieved. The oriented cavities in the stress direction along with the deformation of the matrix are shown in Figure 10(d). The plastic deformation, occurring via the debonding process, was the important energy-dissipation process and led to a toughened polymer blend. With the tensile process, the cracks eventually severed the shear yielding bands. In a

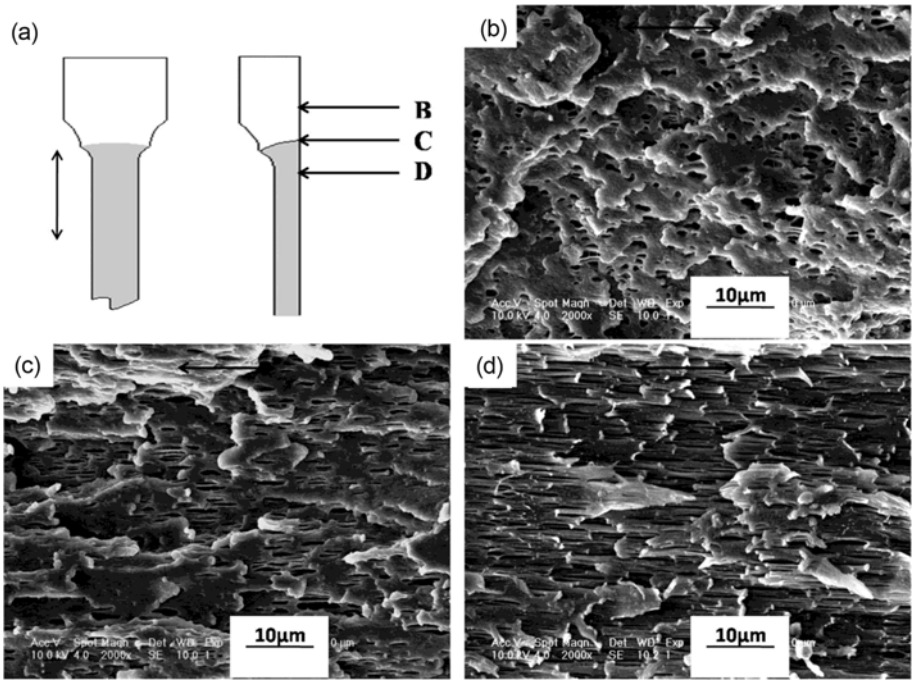


**Figure 10.** (a) Schematic diagram of the measurement locations B, C, and D of the SEM micrographs of the PBT/TPU blend (80/20) during the tensile testing, (b) morphology in region B, (c) morphology in region C, and (d) morphology in region D.

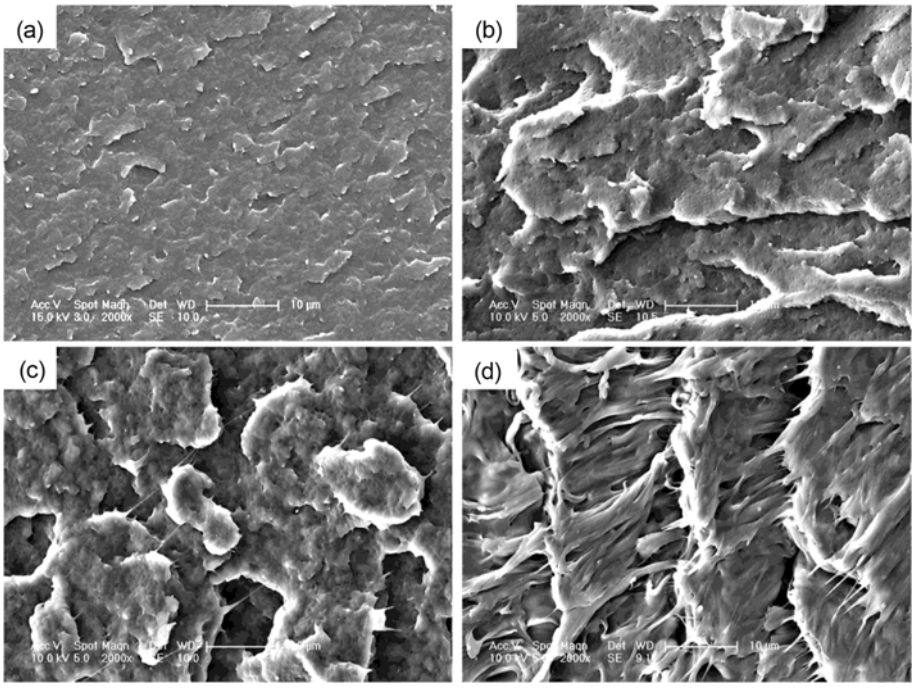


**Figure 11.** SEM micrographs of the fracture surface of PBT/TPU blends; (a) 100/0, (b) 90/10, (c) 80/20, and (d) 70/30.

word, the PBT matrix demonstrated shear yielding during the tensile test, which contributed to the large elongation at break.

To further confirm the toughening mechanism of PBT/TPU blends, the impact-fracture surfaces were also observed by SEM, the micrographs are shown in Figure 11. In Figure 11(a) neat PBT showed a relatively smooth surface with a few failed fibers, indicating a typical brittle fracture behavior. With addition of 10-20 wt% TPU, the fractured surfaces exhibited more evidence of ductile fractures as the fracture surfaces became rougher and some fibrils were observed. The toughening effect in these cases remained moderate. When 30 wt% TPU was added to PBT (Figure 11(d)), the impact caused not only the fibrils but also clear, large scale plastic deformation, which implied shear yielding of the PBT matrix had taken place. The corresponding amount of plastic deformation was high and effectively dissipated the fracture energy, which resulted in the highly improved impact strength.

## Conclusion

The effect on crystallization and mechanical behaviors of a toughened PBT blend was investigated. The results suggested that PBT and TPU were immiscible. The blends had lower crystallinity compared to neat PBT, indicating the possibility that the polymer chains had restricted movement in the blends macrostructure. It was also found that the crystal structure of PBT was not modified by the presence of TPU. Incorporation of TPU elastomer decreased the tensile strength and increased the elongation at break due to the lower modulus and tensile strength of TPU compared to PBT. The 70/30 PBT/TPU blend was super tough and the notched impact strength was about 22 times that of neat PBT. The brittle fracture of neat PBT was gradually transformed into ductile fracture by the addition of the TPU elastomer. SEM results demonstrated that the shear yielding of the PBT matrix and the cavitations of the rubber particles were the major toughening mechanisms.

## References

1. D. K. Yong, H. Y. Jeon, J. J. Yoo, J. N. Im, and S. G. Lee, *Fiber. Polym.*, **14**, 1422 (2013).
2. D. Nabi Saheb and J. P. Jog, *Adv. Polym. Tech.*, **19**, 41 (2009).
3. Y. Guo, J. X. He, X. N. Zhang, S. L. Sun, and H. X. Zhang, *J. Macromol. Sci., Part B. Phys.*, **54**, 823 (2015).
4. S. L. Sun, F. F. Zhang, Y. Fu, C. Zhou, and H. X. Zhang, *J. Macromol. Sci. Part B. Phys.*, **52**, 861 (2013).
5. M. E. J. Dekkers, S. Y. Hobbs, and V. H. Watkins, *Polymer*, **32**, 2150 (1991).
6. A. N. Wilkinson, S. B. Tattum, and A. J. Ryan, *Polymer*, **38**, 1923 (1997).
7. D. C. Wahrmund and D. R. Paul, *J. Appl. Polym. Sci.*, **22**, 2155 (1978).
8. D. Delimoy, C. Bailly, J. Devaux, and R. Legras, *Polym. Eng. Sci.*, **28**, 104 (1988).

9. C. C. Huang and F. C. Chang, *Polymer*, **38**, 2135 (1997).
10. V. M. Nadkarni, V. L. Shingankuli, and J. P. Jog, *Polym. Eng. Sci.*, **28**, 1326 (1988).
11. J. An, J. Y. Ge, and Y. X. Liu, *J. Appl. Polym. Sci.*, **60**, 1803 (1996).
12. J. Jang and J. Won, *Polymer*, **39**, 4335 (1998).
13. A. S. Liu, W. B. Liau, and W. Y. Chiu, *Macromolecules*, **31**, 6593 (1998).
14. L. Finelli, N. Lotti, and A. Munari, *Eur. Polym. J.*, **37**, 2039 (2001).
15. E. Hage, W. Hale, H. Keskkula, and D. R. Paul, *Polymer*, **38**, 3237 (1997).
16. W. Hale, J. H. Lee, H. Keskkula, and D. R. Paul, *Polymer*, **40**, 3621 (1999).
17. W. Hale, H. Keskkula, and D. R. Paul, *Polymer*, **40**, 365 (1999).
18. R. Sharma and S. N. Maiti, *Polym. Eng. Sci.*, **53**, 2242 (2013).
19. X. H. Wang, H. X. Zhang, Z. G. Wang, and B. Z. Jiang, *Polymer*, **38**, 1569 (1997).
20. A. Cecere, R. Greco, G. Ragosta, G. Scarinzi, and A. Taglialatela, *Polymer*, **31**, 1239 (1990).
21. N. M. Larocca, E. Hage, and L. A. Pessan, *Polymer*, **45**, 5265 (2004).
22. N. M. K. Lamba, K. A. Woodhouse, and S. L. Cooper, "Polyurethanes in Biomedical Applications", p.277, CRC Press, Boca Raton, FL, 1998.
23. P. A. Gunatillake, G. F. Meijs, S. J. McCarthy, and R. Adhikari, *J. Appl. Polym. Sci.*, **76**, 2026 (2000).
24. A. Simmons, J. Hyvarinen, and L. Poole-Warren, *Biomaterials*, **27**, 4484 (2006).
25. S. Gogolewski, K. Gorna, and A. S. Turner, *J. Biomed. Mater. Res. Part A.*, **77**, 802 (2006).
26. C. Hepburn, "Polyurethane Elastomers", p.249, Applied Science, London, 1982.
27. R. W. Seymour, G. M. Estes, and S. L. Cooper, *Macromolecules*, **3**, 579 (1970).
28. C. M. Brunette, S. L. Hsu, and W. J. MacKnight, *Macromolecules*, **15**, 71 (1982).
29. O. Olabisi, "Handbook of Thermoplastics", p.299, Marcel Dekker, New York, 1997.
30. K. Palanivelu, P. Sivaraman, and M. Dasaratha Reddy, *Polym. Test.*, **21**, 345 (2002).
31. K. P. Gallagher, X. Zhang, and J. P. Runt, *Macromolecules*, **26**, 588 (1993).
32. W. L. Li, J. L. Liu, C. W. Hao, K. Jiang, D. F. Xu, and D. J. Wang, *Polym. Eng. Sci.*, **48**, 249 (2008).
33. K. H. Illers, *Coll. Polym. Sci.*, **258**, 117 (1980).
34. S. L. Sun, Z. C. Chen, Z. Y. Tan, C. Zhou, M. Y. Zhang, and H. X. Zhang, *e-polymers*, **142**, 1 (2007).
35. C. F. Pratt and S. Y. Hobbs, *Polymer*, **17**, 12 (1976).
36. I. H. Hall, "Structure of Crystalline Polymers", p.39, Elsevier Applied Science, London, UK, 1984.
37. Z. S. Mo and H. F. Zhang, *J. Macromol. Sci. Rev. Macromol. Chem. Phys.*, **C35**, 555 (1995).
38. J. H. Yin and Z. S. Mo, "Modern Polymer Physics", p.477, Science Press, Beijing, 2001.
39. Q. X. Zhang, Z. S. Mo, S. Y. Liu, and H. F. Zhang, *Macromolecules*, **33**, 5999 (2000).
40. C. H. Macgillavry and G. D. Rieck, "International Tables for X-ray Crystallography", pp.101-108, Kynoch: Birmingham, AL, 1974.
41. H. L. Zhang, X. H. Sun, Q. Y. Chen, M. Q. Ren, Z. H. Zhang, H. F. Zhang, and Z. S. Mo, *Chinese J. Polym. Sci.,* **25**, 589 (2007).
42. H. Tsuji, K. Ikarashi, and N. Fukuda, *Polym. Degrad. Stab.*, **84**, 515 (2004).
43. F. Yang, Z. B. Qiu, and W. T. Yang, *Polymer*, **50**, 2328 (2009).
44. R. M. Taib, Z. A. Ghaleb, and Z. A. M. Ishak, *J. Appl. Polym. Sci.*, **123**, 2715 (2012).
45. S. Wu, *Polymer*, **26**, 1855 (1985).
46. A. J. Kinloch and R. J. Young, "Fracture Behaviour of Polymers", pp.421-471, Applied Science Publisher, New York, 1983.
47. G. M. Kim and G. H. Michler, *Polymer*, **39**, 5689 (1998).
48. Z. H. Liu, X. G. Zhu, L. X. Wu, Y. Li, Z. N. Qi, C. Choy, and F. Wang, *Polymer*, **42**, 737 (2001).